IEEE Photonics Journal
An IEEE Photonics Society Publication

Open Access

Carrier Dynamics in High-Efficiency Blue GaN Light-Emitting Diodes Under Different Bias Currents and Temperatures

Volume 4, Number 5, October 2012

Kai-Lun Chi
Jin-Wei Shi
C. H. Jang
Pyry Kivisaari
Jani Oksanen
Jukka Tulkki
M. L. Lee
J. K. Sheu

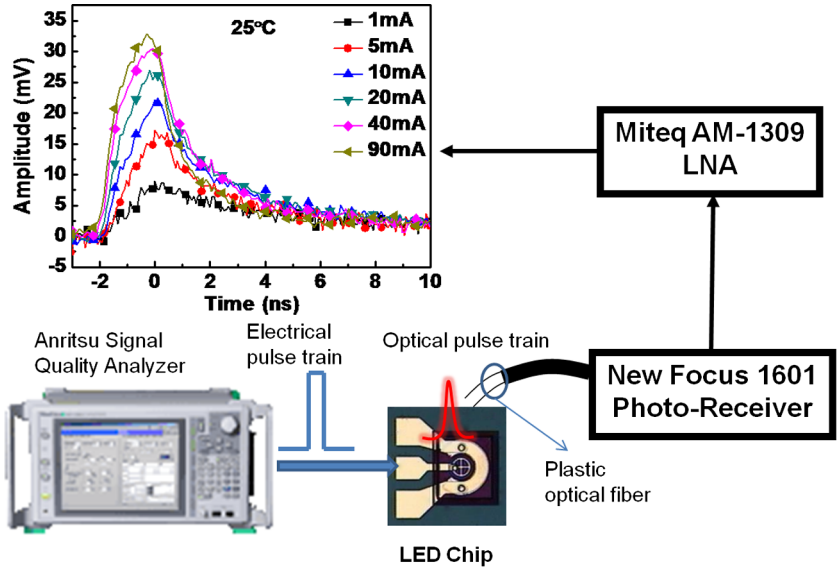

DOI: 10.1109/JPHOT.2012.2217947
1943-0655/$31.00 ©2012 IEEE

Carrier Dynamics in High-Efficiency Blue GaN Light-Emitting Diodes Under Different Bias Currents and Temperatures

Kai-Lun Chi,[1] Jin-Wei Shi,[1] C. H. Jang,[2] Pyry Kivisaari,[3] Jani Oksanen,[3] Jukka Tulkki,[3] M. L. Lee,[4] and J. K. Sheu[2]

[1]Department of Electrical Engineering, National Central University, Taoyuan 320, Taiwan
[2]Department of Photonics and Advanced Optoelectronic Technology Center, National Cheng Kung University, Tainan City 70101, Taiwan
[3]Department of Biomedical Engineering and Computational Science, Aalto University, 00076 Aalto, Finland
[4]Department of Electro-Optical Engineering, Southern Taiwan University, Tainan City 71001, Taiwan

DOI: 10.1109/JPHOT.2012.2217947
1943-0655/$31.00 ©2012 IEEE

Manuscript received August 23, 2012; revised September 1, 2012; accepted September 4, 2012. Date of publication September 7, 2012; date of current version September 26, 2012. This work was supported in part by the Bureau of Energy, Ministry of Economic Affairs of Taiwan, through Grant 100-D0204-6, by the LED Lighting Research Center of NCKU, and by the National Science Council under Grants NSC 98-2221-E-218-005-MY3, 100-2112-M-006-011-MY3, 100-3113-E-006-015, 96-2221-E-008-106-MY3, and 97-2221-E-006-242-MY3. Corresponding author: J.-W. Shi (e-mail: jwshi@ee.ncu.edu.tw).

Abstract: Distinct temperature-dependent dynamic behaviors of GaN-based blue light-emitting diodes (LEDs) are observed by use of the very-fast electrical–optical pump-probe technique. Our static and impulse response measurement results indicate that the behaviors of internal carrier dynamics under different ambient temperatures can be classified into three regimes covering a wide range of bias current densities (20–2000 A/cm^2). The first regime is when the bias current density ranges from low to moderate (20–100 A/cm^2). The measured external quantum efficiency (EQE) degrades dramatically from 57 to 44%, and the measured waveform and extracted time constants of measured impulse responses are invariable from room temperature (RT) to 200 °C, which indicates that the carrier leakage is not an issue for the observed droop phenomenon. When the bias current density further increases to near 1 kA/cm^2, the droop phenomenon are mitigated (44 to 24%). However, a significant shortening of the measured impulse response happens under 200 °C operation due to the device-heating effect. This phenomenon is diminished when the bias current densities are further increased to over 1 kA/cm^2, due to the screening of the piezoelectric field. The extracted time constants can also be used to explain the droop phenomenon in GaN LED under high bias currents.

Index Terms: Light-emitting diodes (LEDs).

1. Introduction

Gallium nitride (GaN)-based blue or violet light-emitting diodes (LEDs) have attracted a lot of attention in recent years [1] due to their strong potential in the next-generation solid-state lighting. In order to further improve their performance and meet such challenge, a number of theoretical and experimental studies have been carried out in order to better understand the internal carrier dynamics inside InGan/GaN multiple quantum wells (MQWs) and the origin of the efficiency droop during operation of GaN-based blue LEDs [2]–[12]. Several measurement techniques and possible mechanisms have been proposed to investigate and explain the external quantum efficiency (EQE) droop phenomenon in GaN-based green and blue LEDs, such as defect recombination [4], carrier

overflow and leakage [2], [5], the (direct or indirect) Auger effect [6]–[12], and piezoelectric (PZ)-field induced carrier leakage [12], [13]. In these reported works, the internal carrier dynamics is usually analyzed based on the extracted external and internal quantum efficiency of the blue LEDs and the technique of differential carrier lifetime measurement [2], [5], [9], [10]. However, the internal carrier dynamics, which occurs during the operation of GaN LEDs, cannot be so straightforwardly characterized with these approaches. In this paper, for the first time, we adopted the fast electrical–optical (E–O) pump-probe technique [11], [12] to directly characterize the internal carrier dynamics of a GaN-based high-efficiency blue LED (maximum absolute EQE: 57%) under an extremely wide range of bias currents (20 to 2000 A/cm^2) and ambient temperatures (room temperature (RT) to 200 °C). In such scheme, a short electrical pulse ($\sim$ ps) is injected into the fast GaN LED during operation, after which we can then measure its output optical pulses by use of high-speed photoreceiver circuits [11]. Here, the fast GaN LED with a miniaturized device active area is necessary to avoid the influence of its *RC*-delay time on the measured responses [11], [12]. These measured impulse responses from the LED are thus expected to represent information about the carrier dynamics inside it without any assumption on carrier recombination processes [2], [5], [9], [10]. Furthermore, another advantage of this demonstrated technique compared with the ultrafast optical pump-probe technique [14] is that an electrical pulse (instead of an optical pulse) is used to excite the device, which matches the case of forward-bias LEDs with electrical signal injection. Recently, such proposed measurement technique (E–O pump probe) has also been used to study the dynamic behavior of photonic-crystal-based miniaturized LED [15]. In addition, most studies of III-nitride LED droop focus on current densities near the maximum efficiency [2]–[10]. Our work is intended to serve as a reference for studying the droop at different temperatures at extremely high current densities ($\sim$ 2 kA/cm^2) due to the miniaturized size of our device. Our static and dynamic measurement results indicate that the temperature-dependent dynamic behaviors of studied device can be classified into three regimes covering a wide range of bias current densities due to the influence of PZ field on the active region. In the low-to-moderate bias current range (20–100 A/cm^2), the EQE degrades dramatically from 57% to 44%, and the measured E–O impulse responses are insensitive to the ambient temperature (up to 200 °C). This is the evidence that such EQE droop phenomenon is not due to the additional loss mechanisms induced by high temperature. When the bias current density further tremendously increases from $>$ 100 A/cm^2 to near 1 kA/cm^2, the droop phenomenon begins to be mitigated (44% to 24%) because both the spontaneous and nonradiative recombination processes become saturated [9]. Under this bias regime, when the ambient temperature reaches 200 °C, the measured E–O impulse responses shortens significantly, accompanying a serious degradation in output optical power. This suggests that the device-heating induced carrier leakage would be one of the important issues to the droop phenomenon under such high-temperature operation. Finally, when the bias current density becomes extremely high (1 to 2 kA/cm^2), the degradation in EQE is further mitigated (24% to 16%). At 200 °C, the device-heating phenomenon is diminished due to the screening of the PZ field by injected carriers and the increase in effective barrier height [11], [12] of active layers. Under this bias regime, the saturation of spontaneous and nonradiative recombination processes may eventually dominate the droop phenomenon.

2. Device Structure

The top view of the fabricated device and its epilayer structures are shown in Fig. 1(a) and (b), respectively. As can be seen in Fig. 1(b), the structures were grown on a (0001) sapphire substrate, mainly composed of 17 pairs of $In_{0.18}Ga_{0.82}N$/GaN MQWs. Details of the doping density and thickness of each layer in the structure are specified. As can be seen, the six pairs of MQWs, which neighbor the n-side cladding layers, have n-type doping in their barrier layers. On the other hand, the remaining 11 pairs of MQWs are undoped. It has been demonstrated that this type of partial n-type doping structure will greatly improve the output power, differential resistance, and modulation speed of the LEDs; for more information, see our previous work [16], [17]. Carrier leakage can be avoided by inserting the two $Al_{0.12}Ga_{0.95}N$ layers near the p- and n-type cladding layers [5].

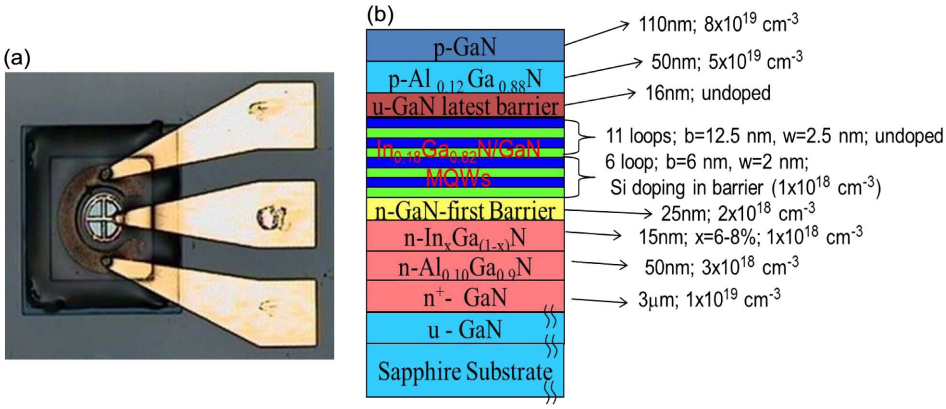

Fig. 1. (a) Top view of the demonstrated LED; (b) conceptual cross-section view of our device. b: barrier, w: well, u: un-doped.

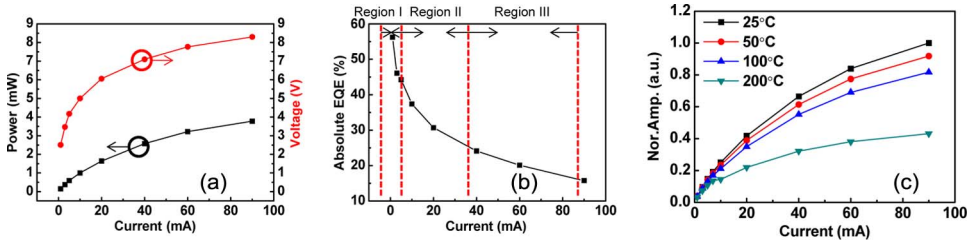

Fig. 2. (a) Measured output power and voltage of LED versus bias current; (b) extracted EQE versus bias current of LED; (c) variation of the measured output power for the same device versus bias current under four different ambient temperatures (25 °C, 50 °C, 100 °C, and 200 °C).

A 15-nm-thick n-type $In_xGa_{1-x}N$ layer (doping density of 1×10^{18} cm^{-3}) with a mole fraction x $(x = 6{-}8\%)$, much less than that of the blue MQW layers, was inserted between the bottom n-GaN layer and the active MQW layers. The benefit to the bottom current spreading and improvement in the current–voltage (*I–V*) characteristics in the fabricated LEDs can be attributed to the narrower band gap, high doping density, and possible lower resistivity of the inserted InGaN layer compared with that of the bottom n-GaN layer [18], [19]. As can be seen in Fig. 1(a), the fabricated device has an active diameter of 75 μm, and it is integrated with a coplanar waveguide (CPW) pads for on-wafer high-speed measurement. Our device size is much smaller than that of the typical commercial blue LED for solid-state lighting, which usually has an active area around 300×300 μm^2. We adopted such a miniaturized device size in our experiments for the purpose of relaxing the *RC*-limited bandwidth of the LED and eliminating the influence of the *RC*-delay time on the measured E–O impulse responses [11], [12]. This ensures that our measured traces truly represent the internal carrier dynamics instead of the external device *RC* delay time. For details of the LED fabrication processes, please refer to our previous work [19], [20].

3. Measurement Results and Discussion

Fig. 2(a) shows the measured output power and bias voltage of our device versus the bias current under RT. According to the measured output power versus bias current, as shown in Fig. 2(a), we can further extract the EQE versus bias current of our device, as shown in Fig. 2(b). Fig. 2(c) shows the measured static output power (after normalization) versus bias current under different ambient temperatures. A well-calibrated integrating sphere was adopted for these power measurements. As can be seen in Fig. 2(b), under low bias current operation (< 10 mA), the measured EQE could be

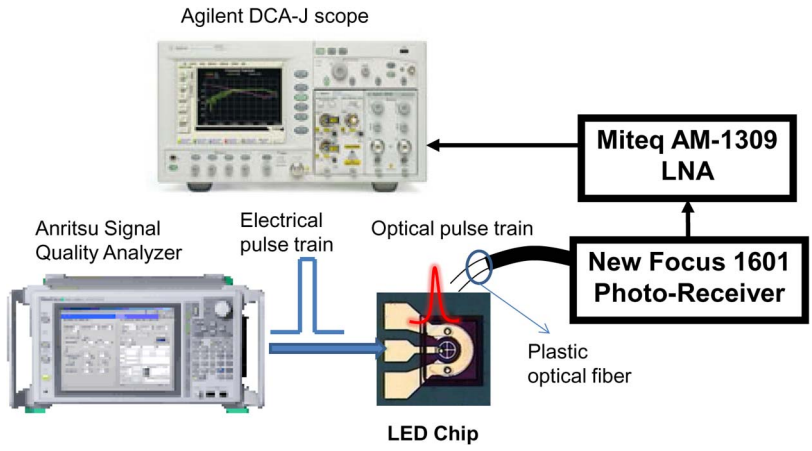

Fig. 3. Setup for E–O pump-probe measurement. LNA: low noise amplifier.

as high as ∼50%. In this bias regime, the corresponding bias current density is around 200 A/cm^2, which is close to the bias current density of GaN-based blue LEDs required for high-power operation [7].

Under such bias current density, the corresponding junction temperature of GaN-based LED is usually at around 120 °C [21]. Such temperature is even lower than the highest ambient temperature (200 °C) during our static [as shown in Fig. 2(c)] and dynamic measurements (as discussed latter). We can thus conclude that, under such operation condition, the junction temperature of our device is close to the ambient temperature when it is over 100 °C. However, if we further increase the bias current density [regions II and III in Fig. 2(b)], the junction temperature might be eventually higher than the ambient temperature. Compared with the values reported for high-performance blue LEDs under the same bias current density (∼200 A/cm^2), our achieved value of EQE is even higher (∼40% versus 30% [7]). However, we can see that it degrades dramatically with the increase of bias current (density). The relation between the bias current density and the EQE, as shown in Fig. 2(b), is highly nonlinear and can be roughly classified into three regions (I, II, and III) with different slopes of the fitting lines of EQE versus bias current, as specified in Fig. 2(a).

In order to characterize the different mechanisms for EQE droop and internal carrier dynamics in these three regimes and for a wider range of bias current densities (20 to 2000 A/cm^2) tested, we performed E–O impulse response measurement under different bias currents and ambient temperatures. Compared with the static measurement results, by use of our dynamic measurement technique, we can directly extract the recombination time constants in the active layers (InGaN/GaN MQWs) of LED under different operation conditions (current and temperatures). Furthermore, the extracted time constants would be useful in the theoretical analysis of static and dynamic behaviors of GaN-based lasers and LEDs [22].

A conceptual diagram of the E–O pump-probe measurement setup was given in Fig. 3 [11], [12]. During measurement, the device under testing (DUT) was mounted on a hot plate for temperature-dependent measurement then injected with different dc bias currents. An electrical pulse train with a full width at half-maximum (FWHM) of around 100 ps, a 1/64 duty cycle, and a fixed 2-V peak output voltage was generated by a programmable pulse pattern generator (Anritsu MP1800A series) and injected into the device for impulse response measurement.

We have also tried to inject our device with an even shorter electrical pulse, but the measured impulse response showed no significant change. This result indicates that the injected electrical pulsewidth was much faster than the internal response time of the LED inside. The optical pulse generated from the DUT was collected by high-speed photoreceiver circuits with a 3-dB bandwidth of approximately 1.5 GHz (New Focus, 1601-AC). This was connected to a 1.5-GHz 3-dB low-noise amplifier (LNA, Miteq AM-1309) with a high-speed sampling scope (Agilent DCA-J scope) to record the impulse response.

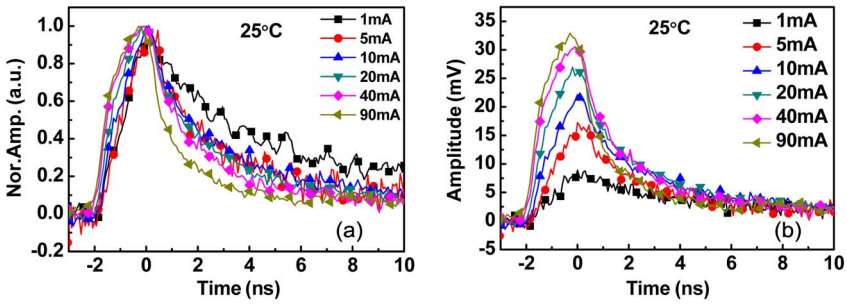

Fig. 4. Measured impulse responses for our device under different bias currents at RT (a) with and (b) without normalization.

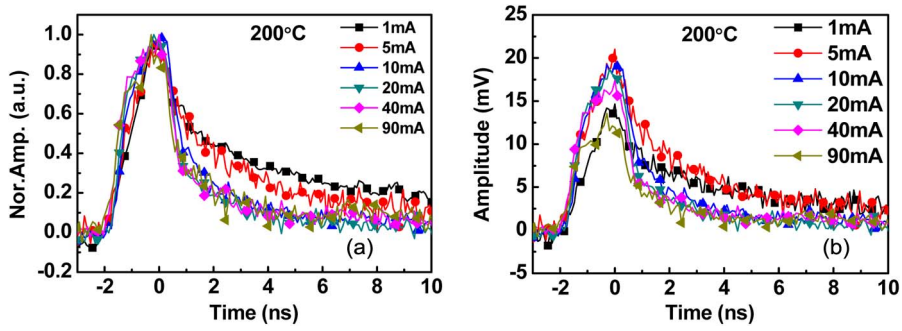

Fig. 5. Measured impulse responses for our device under different bias currents at 200 °C (a) with and (b) without normalization.

Figs. 4 and 5 show the measured impulse responses of our device for different bias currents with/without normalization, at RT and 200 °C, respectively. As can be seen in these two figures, the measured pulsewidths of impulse response significantly shorten from 4 to 2 ns when the dc bias current increases from 1 to 90 mA, accompanied by a increase in the peak amplitudes. However, in Fig. 4(b), when the bias current exceeds 40 mA, significant saturation of the peak amplitude can be observed. The measured traces in Fig. 5(b) show a similar trend.

When the ambient temperature reaches 200 °C, the increase in bias current (> 40 mA) even leads to the significant degradation in the peak amplitude. Based on these measurement results, we can thus conclude that the shortening of the measured impulse responses, especially under a high bias current (> ∼40 mA), is due to the enhancement of the nonradiative recombination process (degradation of EQE) that accompanies the increase of the bias current at these two measuring temperatures. We will discuss this issue in greater detail later. Furthermore, compared with the traces measured at RT [shown in Fig. 4], the traces measured at 200 °C (see Fig. 5) show significant degradation in amplitude. This result indicates a serious degradation in EQE for our device under 200 °C operation. As shown in Fig. 2(c), we can see that there is a serious degradation (∼50% degradation in output power compared with that of under RT operation) in the measured output power at 200 °C when the bias current exceeds around 40 mA, which is consistent with the dynamic measurement results shown in Fig. 5. In order to clearly investigate the mechanism leading to EQE droop in the three different bias current density regimes, as indicated in Fig. 2(b), we performed temperature-dependent E–O impulse response measurement in all three bias regimes.

Fig. 6(a) to (d) shows the temperature-dependent E–O impulse responses (RT to 200 °C) measured under 1-, 3-, 5-, and 7-mA bias currents, respectively. Each trace is normalized to its maximum for easy comparison. These bias current densities correspond to that of region I (20 to ∼100 A/cm^2), as shown in Fig. 2(b). As can be seen, in this bias current regime, the measured E–O impulse responses are insensitive to the variation in ambient temperature even when it reaches

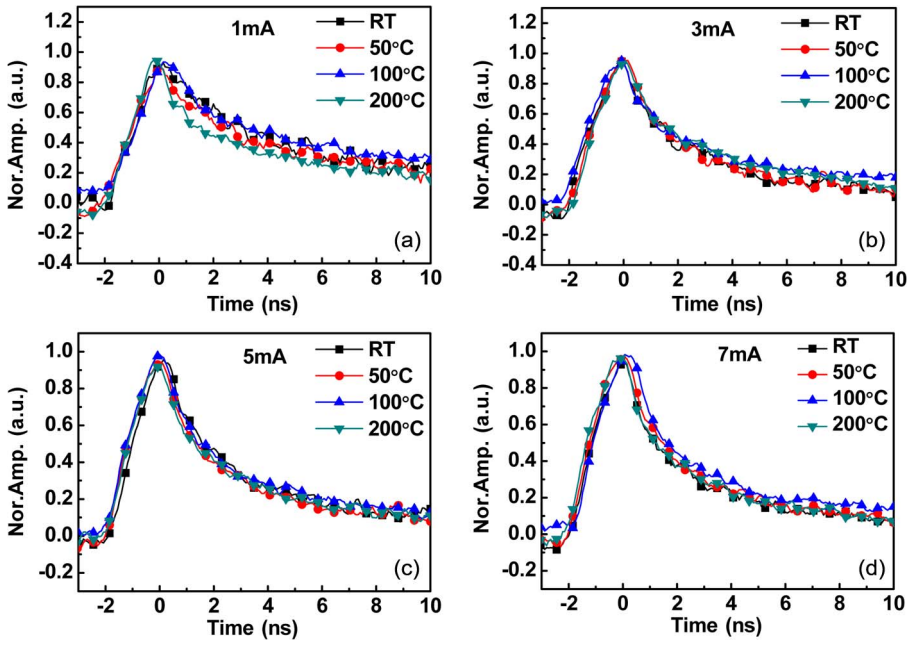

Fig. 6. Measured impulse responses for the device (after normalization) under different ambient temperatures (25 °C, 50 °C, 100 °C, and 200 °C) and a fixed bias current at (a) 1, (b) 3, (c) 5, and (d) 7 mA.

200 °C. This result possibly indicates that additional loss mechanisms induced by high temperature, most probably temperature-related carrier leakage, is not the reason for the observed dramatic EQE droop in this regime, which is consistent with the static power measurement result. As can be seen in Fig. 2(c), under such a low bias regime (1 to 7 mA), there is no significant degradation in the output power. This is because device-heating phenomenon is not an issue with such a low bias current.

Fig. 7(a) to (c) shows the temperature-dependent E–O impulse responses (RT to 200 °C) measured under 10-, 20-, and 40-mA bias currents, respectively. Each trace is normalized to its maximum for easy comparison. These bias currents densities (200 to 1000 A/cm^2) correspond to those in region II, as specified in Fig. 2(b). As can be seen, in this bias current regime, there is great shortening of the measured E–O impulse responses when the ambient temperature reaches 200 °C, accompanied by a serious degradation in the output power, as shown in Fig. 2(c). This result suggests that device-heating induced carrier leakage has an important contribution to the EQE droop at such a high ambient temperature (200 °C) and bias current regime. Nevertheless, there is no significant carrier leakage induced shortening of the impulse response or degradation in output power [as shown in Fig. 2(c)] measured at other temperatures lower than 200 °C. We can thus conclude that, under RT operation, both the saturation of the radiative spontaneous recombination and the nonradiative recombination [9], [10] still dominate the droop phenomenon, according to the extracted fall-time constants of the impulse responses to be discussed later.

Fig. 8(a) and (b) shows the measured temperature-dependent E–O impulse responses (RT to 200 °C) for extremely high bias currents (densities) of 60 and 90 mA (1.3 and 2 kA/cm^2), respectively. We can clearly see that the impulse response becomes invariant when the increase in ambient temperature. This is similar to the traces measured in region I and can be attributed to the fact that, under such a high bias current density, the strong PZ field inside the GaN/InGaN MQW region can be completely screened by the space-charge field induced by the external injected current. The screened PZ field consequently increases the effective barrier height in the MQW region [12], [23], [24]. This should be accompanied by a lower probability of carrier escape and less output power degradation under high-temperature operation. In this high bias current regime, the

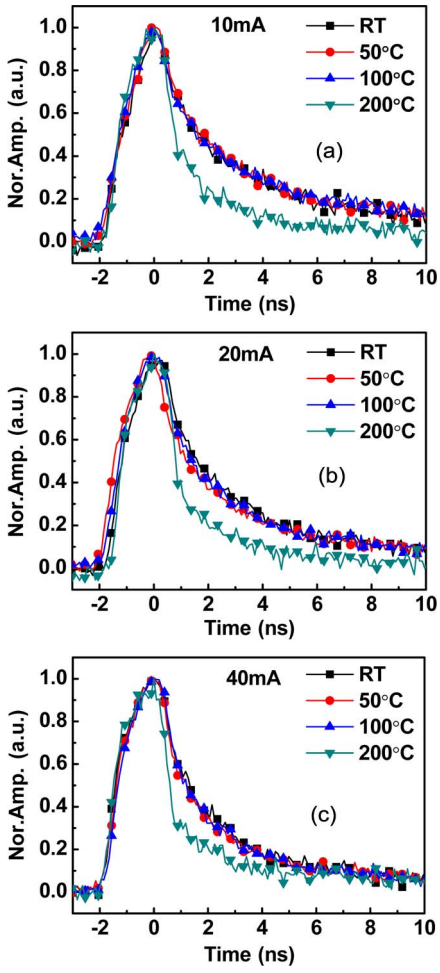

Fig. 7. Measured impulse responses for the device (after normalization) under different ambient temperatures (25 °C, 50 °C, 100 °C, and 200 °C) and a fixed bias current at (a) 10, (b) 20, and (c) 40 mA.

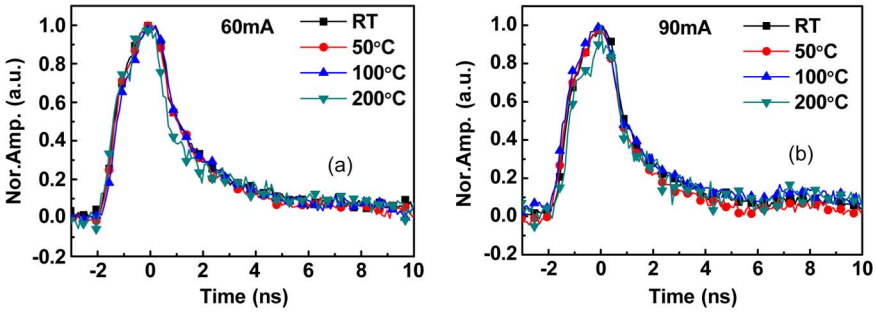

Fig. 8. Measured impulse responses for the device (after normalization) under different ambient temperatures (25 °C, 50 °C, 100 °C, and 200 °C) and a fixed bias current at (a) 60 and (b) 90 mA.

droop phenomenon begins to be mitigated and is eventually dominated by the saturation of spontaneous recombination.

By analyzing the fall-time constants of these measured impulse responses, we can further distinguish which mechanism possibly dominates the droop phenomenon in the different bias current regimes. The fall-time constants, which can be extracted from these measured impulse responses

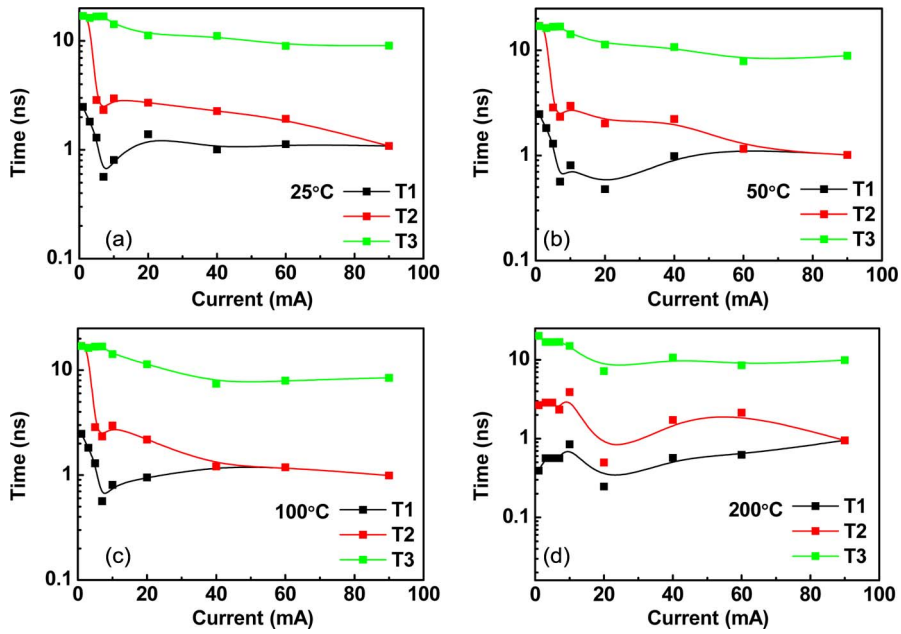

Fig. 9. Extracted τ_r (fall time constants) for measured impulse responses versus bias currents under (a) 25 °C, (b) 50 °C, (c), 100 °C, and (d) 200 °C operation.

by use of a simple exponential decay function with several fall-time constants, represent the recombination time (τ_r) of the internal carrier inside the active MQW layers. This is because the *RC*-delay time is not an issue in our LEDs with their miniaturized active area. The adopted fitting equation is given as follows:

$$\left(A_1 \times e^{\frac{-t}{T_1}} + A_2 \times e^{\frac{-t}{T_2}} + A_3 \times e^{\frac{-t}{T_3}}\right). \quad (1)$$

where the values of amplitude constants (A_1 to A_3) and time constants (T_1 to T_3) can be adjusted to fit the fall-time traces of measured impulse responses. Fig. 9(a) to (d) show the extracted time constants (T_1 to T_3) versus bias current (1 mA to 90 mA) under 25 °C, 50 °C, 100 °C, and 200 °C operations, respectively. The corresponding bias current density ranges between 20 to 2000 A/cm^2.

As can be seen, the slowest time constant T3, which has a value of over 10 ns, remains almost invariant with the bias current density and ambient temperature. Given the measured bias current densities, this should not be the reason for the observed droop phenomenon, which varies significantly with the bias current, as discussed. The other two time constants (T1 and T2) change significantly with the bias current and ambient temperature. When the bias current density increases, there is the most significant reduction in T2 among the three time constants. For example, there is a dramatic reduction from 17 to 2.8 ns when the bias current increases from 1 to 5 mA, which can help to explain the observed serious droop phenomenon in this bias regime, as illustrated in Fig. 2(b). From the superlinear increase in the inverse of T2 with the bias current (injected carrier density) in this low bias regime, we may conclude that the extracted T2 is possibly a nonradiative Auger recombination time constant, which dominates the EQE droop phenomenon in region I (20–100 A/cm^2) [8]–[10]. On the other hand, the inverse to T1 increases almost linearly with the bias current (injected carrier density) but shows a reduction when the ambient temperature reaches 200 °C in a certain bias current range [region II, as indicated in Fig. 2(b)]. Such a time constant may represent the mixing of radiative spontaneous recombination and nonradiative device-heating induced carrier leakage time constants. Under 200 °C operations, the reduction in T1 implies an enhancement in the device-heating induced carrier leakage rate, which is accompanied by serious degradation in the EQE, as illustrated in Fig. 2(c). Furthermore, under RT to 100 °C operation, after

the bias current density increases further to over $\sim$100 A/cm^2 (20 mA), there is no change in the values of T1 but is pinned at around 1 ns. This trend is similar to the dynamic measurement results reported for GaN-based blue LEDs based on the differential carrier lifetime analysis technique [9]. In such reported work [9], the extracted spontaneous radiative recombination time constant shows significant pinning at the value around ($\sim$3 ns) when the bias current exceeds 300 A/cm^2. This can be explained by the saturation of spontaneous recombination (phase-space filling effect) [9]. On the other hand, under 200 °C operation, the time for the pinning of spontaneous recombination happens at a higher bias current (over 60 mA), because a higher bias current is required to minimize the device-heating induced carrier leakage, as indicated in Figs. 8 and 9.

It is also important to note that our measurements presented here indicated the importance of multiple carrier lifetimes (T1 to T3) in fitting the carrier dynamics in InGaN QWs. By using these results, we analyzed the various recombinations of the carriers in the QWs, as discussed. These results are useful for providing insights in carrier dynamics in InGaN QWs, but our interpretation of these results may require a more detailed analysis for confirmation. It is important to note the possible importance of other mechanisms such as carrier leakages and thermionic carrier escape process in GaAs-based lasers [25]–[27] and InGaN-based LEDs [22], [28]–[30], which may also be applied to explain the observed phenomenon here. The general theory of current injection efficiency in QW lasers or LEDs shows the existence of thermionic carrier escape in QW leads to suppression of current injection efficiency at high current density [25], and the suppression of thermionic carrier escape in QW lasers have led to the realization of high-performance lasers at high temperature [25]–[27]. The importance of thermionic carrier escape in QW LEDs has been extended to explain the carrier leakages, and reduction in current injection and internal quantum efficiencies for InGaN QW LEDs [22], [28]–[30]. Furthermore, recent works have pointed the need of using multiple carrier recombination rates in fitting the carrier dynamics in InGaN QWs, which are attributed to the carrier recombination in both extended and localized states in the QW [31], [32].

Although there are lots of other possible mechanisms to explain our observed results as the above discussion, our extracted T1 (spontaneous recombination time constant) is really much smaller in value (1 versus 3 ns) than that reported for GaN-based blue LEDs operated at RT [9], even under the same bias current density. The fast spontaneous emission rate in the InGaN QWs is important for achieving high IQE and EQE in LEDs [33]–[35]. The spontaneous emission rate in InGaN QW is limited by charge separation effect attributed to the existence of the polarization field in the QWs [33]–[35]. Several approaches have been used to suppress the charge separation in InGaN QWs by using nonpolar InGaN QWs [36], [37], polar InGaN QWs with large overlap designs [38]–[41], Type-II MQWs [42], [43], strain-compensated MQW [44], [45], and ternary substrate/template methods [46], [47].

Our measurement results indicate a higher spontaneous recombination rate in our active layers so that a superior EQE performance to that reported for blue LEDs can thus be measured, as shown in Fig. 2(a). In addition, when the bias current further increases to over 1 kA/cm^2, the values of the extracted T1 and T2 time constants both merge together to be pinned at around 1 ns, which is close to the extracted Auger recombination time in GaN-based blue LEDs under the same bias current density ($\sim$1 kA/cm^2) [9]. This explains the mitigation of the droop phenomenon in regions II and III, which is due to the fact that the nonradiative Auger recombination rate (time) cannot further increase (decrease) with the bias current.

4. Conclusion

In this paper, we directly characterize the internal carrier dynamics inside InGaN/GaN-based blue LEDs during operation using a very fast electro-optical pump-probe technique. The influence of the *RC*-delay time on the measured responses is eliminated by adopting a miniaturized LED structure in our experiments. Overall, from these static and dynamic measurement results, we can conclude that the superior EQE performance of our demonstrated device to that reported for blue LEDs is mainly due to its short radiative recombination time ($\sim$1 ns), as well as the high spontaneous recombination rate. Furthermore, the distinct temperature-dependent behaviors of the E–O impulse

response measured under different bias current densities is due to the influence of the strong PZ field inside the InGaN/GaN MQW layers. These temperature-dependent measurement results suggest that the device-heating induced carrier leakage plays an important role only when the ambient temperature reaches 200 °C and for a certain range of bias currents (100 to 1000 A/cm^2, region II). Under a lower (region I) or higher (region III) bias current density, carrier leakage is not an issue for the droop phenomenon as a consequence of the negligible device-heating effect and the screening of PZ field by injected carriers, respectively.

References

[1] D. A. Steigerwald, J. C. Bhat, D. Collins, R. M. Fletcher, M. O. Holcomb, M. J. Ludowise, P. S. Martin, and S. L. Rudaz, "Illumination with solid state lighting technology," *IEEE J. Sel. Topics Quantum Electron.*, vol. 8, no. 2, pp. 310–320, Mar./Apr. 2002.

[2] M.-H. Kim, M. F. Schubert, Q. Dai, J. K. Kim, E. F. Schubert, J. Piprek, and Y. Park, "Origin of efficiency droop in GaN-based light-emitting diodes," *Appl. Phys. Lett.*, vol. 91, no. 18, pp. 183507-1–183507-3, Oct. 2007.

[3] R. Stevenson, "The LED's dark secret," *IEEE Spectr.*, vol. 46, no. 8, pp. 26–31, Aug. 2009.

[4] J. Hader, J. V. Moloney, and S. W. Koch, "Density-activated defect recombination as a possible explanation for the efficiency droop in GaN-based diodes," *Appl. Phys. Lett.*, vol. 96, no. 22, pp. 221106-1–221106-3, May 2010.

[5] S.-H. Han, D.-Y. Lee, S.-J. Lee, C.-Y. Cho, M.-K. Kwon, S. P. Lee, D. Y. Noh, D.-J. Kim, Y.-C. Kim, and S.-J. Park, "Effect of electron blocking layer in efficiency droop in InGaN/GaN multiple quantum well light-emitting diodes," *Appl. Phys. Lett.*, vol. 94, no. 23, pp. 231123-1–231123-3, Jun. 2009.

[6] Y. C. Shen, G. O. Mueller, S. Watanabe, N. F. Gardner, A. Munkholm, and M. R. Krames, "Auger recombination in InGaN measured by photoluminescence," *Appl. Phys. Lett.*, vol. 91, no. 14, pp. 141101-1–141101-3, Oct. 2007.

[7] N. F. Gardner, G. O. Muller, Y. C. Shen, G. Chen, S. Wantanabe, W. Gotz, and M. R. Krames, "Blue-emitting InGaN-GaN double-heterostructure light-emitting diodes reaching maximum quantum efficiency above 200 A/cm^2," *Appl. Phys. Lett.*, vol. 91, no. 24, pp. 243506-1–243506-3, Dec. 2007.

[8] K. T. Delaney, P. Rinke, and C. G. V. d. Walle, "Auger recombination in nitrides form first principles," *Appl. Phys. Lett.*, vol. 94, no. 19, pp. 191109-1–191109-3, May 2009.

[9] A. David and M. J. Grundmann, "Droop in InGaN light-emitting diodes: A differential carrier lifetime analysis," *Appl. Phys. Lett.*, vol. 96, no. 10, pp. 103504-1–103504-3, Mar. 2010.

[10] E. Kioupakis, P. Rinke, K. T. Delaney, and C. G. V. d. Walle, "Indirect Auger recombination as a cause of efficiency droop in nitride light-emitting diodes," *Appl. Phys. Lett.*, vol. 98, no. 16, pp. 161107-1–161107-3, Apr. 2011.

[11] J.-W. Shi, H.-W. Huang, F.-M. Kuo, W.-C. Lai, M. L. Lee, and J.-K. Sheu, "Investigation of the carrier dynamic in GaN-based cascade green light-emitting-diodes using the very-fast electrical–optical pump-probe technique," *IEEE Trans. Electron Devices*, vol. 58, no. 2, pp. 495–500, Feb. 2011.

[12] J.-W. Shi, F.-M. Kuo, H.-W. Huang, J.-K. Sheu, C.-C. Yang, W.-C. Lai, and M. L. Lee, "The influence of a piezoelectric field on the dynamic performance of GaN-based green light-emitting-diodes with a InGaN insertion layer," *IEEE Electron. Device Lett.*, vol. 32, no. 5, pp. 656–658, May 2011.

[13] M. F. Schubert, J. Xu, J. K. Kim, E. F. Schubert, M. H. Kim, S. Yoon, S. M. Lee, C. Sone, T. Sakong, and Y. Park, "Polarization-matched GaInN/AlGaInN multi-quantum-well light-emitting diodes reduced efficiency droop," *Appl. Phys. Lett.*, vol. 9, no. 4, pp. 041102-1–041102-3, Jul. 2008.

[14] K.-G. Gan, C.-K. Sun, S. P. DenBaars, and J. E. Bowers, "Ultrafast valence intersubband hole relaxation in InGaN multiple-quantum-well laser diodes," *Appl. Phys. Lett.*, vol. 84, no. 23, pp. 4675–4677, Jun. 2004.

[15] G. Shambat, B. Ellis, A. Majumdar, J. Petykiewicz, M. A. Mayer, T. Sarmiento, J. Harris, E. E. Haller, and J. Vučković, "Ultrafast direct modulation of a single-mode photonic crystal nanocavity light-emitting diode," *Nat. Commun.*, vol. 2, no. 539, Nov. 2011, doi: 10.1038/ncomms1543.

[16] J.-W. Shi, H.-Y. Huang, J.-K. Sheu, C.-H. Chen, Y.-S. Wu, and W.-C. Lai, "The improvement in modulation speed of GaN-based light-emitting diode (LED) by use of n-type barrier doping for plastic optical fiber (POF) communication," *IEEE Photon. Technol. Lett.*, vol. 18, no. 15, pp. 1636–1638, Aug. 2006.

[17] J.-W. Shi, J.-K. Sheu, C.-H. Chen, G.-R. Lin, and W.-C. Lai, "High-speed GaN-based green light emitting diodes with partially n-doped active layers and current-confined apertures," *IEEE Electron Device Lett.*, vol. 29, no. 2, pp. 158–160, Feb. 2008.

[18] C.-H. Jang, J.-K. Sheu, C. M. Tsai, S.-J. Chang, W.-C. Lai, M.-L. Lee, T. K. Ko, C. F. Shen, and S. C. Shei, "Improved performance of GaN-based blue LEDs With THE InGaN insertion layer between the MQW active layer and the n-GaN cladding layer," *IEEE J. Quantum Electron.*, vol. 46, no. 4, pp. 513–517, Apr. 2010.

[19] J.-W. Shi, H.-W. Huang, F.-M. Kuo, J.-K. Sheu, W.-C. Lai, and M. L. Lee, "Very-high temperature (200 °C) and high-speed operation of cascade GaN based green light emitting diodes with an InGaN insertion layer," *IEEE Photon. Technol. Lett.*, vol. 22, no. 14, pp. 1033–1035, Jul. 2010.

[20] J.-W. Shi, P-.Y. Chen, C.-C. Chen, J.-K. Sheu, W.-C. Lai, Y.-C. Lee, P.-S. Lee, S.-P. Yang, and M.-L. Wu, "Linear cascade GaN based green light emitting diodes with invariant high-speed/power performance under high-temperature operation," *IEEE Photon. Technol. Lett.*, vol. 20, no. 23, pp. 1896–1898, Dec. 2008.

[21] Y. Xi and E. F. Schubert, "Junction-temperature measurement in GaN ultraviolet light-emitting diodes using diode forward voltage method," *Appl. Phys. Lett.*, vol. 85, no. 12, pp. 2163–2165, Sep. 2004.

[22] H. Zhao, G. Liu, R. A. Arif, and N. Tansu, "Current injection efficiency induced efficiency-droop in InGaN quantum well light-emitting diodes," *Solid State Electron.*, vol. 54, no. 10, pp. 1119–1124, Oct. 2010.

[23] H. Haratizadeh, B. Monemar, P. P. Paskov, J. P. Bergman, B. E. Sernelius, P. O. Holtz, M. Iwaya, S. Kamiyama, H. Amano, and I. Akasaki, "Photoluminescence study of Si-doped GaN/$Al_{0.07}Ga_{0.93}N$ multiple quantum wells with different dopant positions," *Appl. Phys. Lett.*, vol. 84, no. 25, pp. 5071–5073, Jun. 2004.
[24] J. Piprek, R. Farrell, S. P. Denbaars, and S. Nakamura, "Effects of built-in polarization on InGaN-GaN vertical-cavity surface-emitting lasers," *IEEE Photon. Technol. Lett.*, vol. 18, no. 1, pp. 7–9, Jan. 2006.
[25] N. Tansu and L. J. Mawst, "Current injection efficiency of InGaAsN quantum-well lasers," *J. Appl. Phys.*, vol. 97, no. 5, pp. 054502-1–054502-18, Mar. 2005.
[26] N. Tansu, J.-Y. Yeh, and L. J. Mawst, "Experimental evidence of carrier leakage in InGaAsN quantum-well lasers," *Appl. Phys. Lett.*, vol. 83, no. 11, pp. 2112–2114, Sep. 2003.
[27] S. R. Bank, M. A. Wistey, and J. S. Harris, "On the temperature sensitivity of 1.5-μm GaInNAsSb lasers," *IEEE J. Sel. Topics Quantum Electron.*, vol. 11, no. 5, pp. 1089–1098, Sep./Oct. 2005.
[28] J. Wang, L. Wang, L. Wang, Z. Hao, Y. Luo, A. Dempewolf, M. Müller, F. Bertram, and J. Christen, "An improved carrier rate model to evaluate internal quantum efficiency and analyze efficiency droop origin of InGaN based light-emitting diodes," *J. Appl. Phys.*, vol. 112, no. 2, pp. 023107-1–023107-6, Jul. 2012.
[29] I. E. Titkov, D. A. Sannikov, Y.-M. Park, and J.-K. Son, "Blue light emitting diode internal and injection efficiency," *AIP Adv.*, vol. 2, no. 3, pp. 032117-1–032117-4, Sep. 2012.
[30] G.-B. Lin, D. Meyaard, J. Cho, E. F. Schubert, H. Shim, and C. Sone, "Analytic model for the efficiency droop in semiconductors with asymmetric carrier-transport properties based on drift-induced reduction of injection efficiency," *Appl. Phys. Lett.*, vol. 100, no. 16, pp. 161106-1–161106-4, Apr. 2012.
[31] G. Sun, G. Xu, Y. J. Ding, H. Zhao, G. Liu, J. Zhang, and N. Tansu, "Investigation of fast and slow decays in InGaN/GaN quantum wells," *Appl. Phys. Lett.*, vol. 99, no. 8, pp. 081104-1–081104-3, Aug. 2011.
[32] H. Wang, Z. Ji, S. Qu, G. Wang, Y. Jiang, B. Liu, X. Xu, and H. Mino, "Influence of excitation power and temperature on photoluminescence in InGaN/GaN multiple quantum wells," *Opt. Exp.*, vol. 20, no. 4, pp. 3932–3940, Feb. 2012.
[33] R. A. Arif, Y.-K. Ee, and N. Tansu, "Polarization engineering via staggered InGaN quantum wells for radiative efficiency enhancement of light emitting diodes," *Appl. Phys. Lett.*, vol. 91, no. 9, pp. 091110-1–091110-3, Aug. 2007.
[34] R. A. Arif, H. Zhao, Y.-K. Ee, and N. Tansu, "Spontaneous emission and characteristics of staggered InGaN quantum-well light-emitting diodes," *IEEE J. Quantum Electron.*, vol. 44, no. 6, pp. 573–580, Jun. 2008.
[35] J.-H. Ryou, J. Liu, Z. Lochner, H. Kim, S. Choi, H. J. Kim, and R. D. Dupuis, "Control of quantum-confined stark effect in InGaN-based quantum wells," *IEEE J. Sel. Topics Quantum Electron.*, vol. 15, no. 4, pp. 1080–1091, Jul./Aug. 2009.
[36] R. M. Farrell, E. C. Young, F. Wu, S. P. DenBaars, and J. S. Speck, "Materials and growth issues for high-performance nonpolar and semipolar light-emitting devices," *Semicond. Sci. Technol.*, vol. 27, no. 2, pp. 024001-1–024001-15, Feb. 2012.
[37] D. A. Browne, E. C. Young, J. R. Lang, C. A. Hurni, and J. S. Speck, "Indium and impurity incorporation in InGaN films on polar, nonpolar, and semipolar GaN orientations grown by ammonia molecular beam epitaxy," *J. Vac. Sci. Technol. A, Vac. Surf. Films*, vol. 30, no. 4, pp. 041513-1–041513-8, Jul. 2012.
[38] H. Zhao, G. Liu, J. Zhang, J. D. Poplawsky, V. Dierolf, and N. Tansu, "Approaches for high internal quantum efficiency green InGaN light-emitting diodes with large overlap quantum wells," *Opt. Exp.*, vol. 19, no. 4, pp. A991–A1007, Jul. 2011.
[39] H. Zhao, G. Liu, and N. Tansu, "Analysis of InGaN-delta-InN quantum wells for light-emitting diodes," *Appl. Phys. Lett.*, vol. 97, no. 13, pp. 131114-1–131114-3, Sep. 2010.
[40] C.-T. Liao, M.-C. Tsai, B.-T. Liou, S.-H. Yen, and Y.-K. Kuo, "Improvement in output power of a 460 nm InGaN light-emitting diode using staggered quantum well," *J. Appl. Phys.*, vol. 108, no. 6, pp. 063107-1–063107-6, Sep. 2010.
[41] S.-H. Park, J. Park, and E. Yoon, "Optical gain in InGaN/GaN quantum well structures with embedded AlGaNδ layer," *Appl. Phys. Lett.*, vol. 90, no. 2, pp. 023508-1–023508-3, Jan. 2007.
[42] H. Zhao, R. A. Arif, and N. Tansu, "Self-consistent gain analysis of type-II 'W' InGaN-GaNAs quantum well lasers," *J. Appl. Phys.*, vol. 104, no. 4, pp. 043104-1–043104-7, Aug. 2008.
[43] S.-H. Park, D. Ahn, B.-H. Koo, and J.-E. Oh, "Optical gain improvement in type-II InGaN/GaNSb/GaN quantum well structures composed of InGaN/and GaNSb layers," *Appl. Phys. Lett.*, vol. 96, no. 5, pp. 051106-1–051106-3, Feb. 2010.
[44] H. Zhao, R. A. Arif, Y.-K. Ee, and N. Tansu, "Self-consistent analysis of strain-compensated InGaN-AlGaN quantum wells for lasers and light-emitting diodes," *IEEE J. Quantum Electron.*, vol. 45, no. 1, pp. 66–78, Jan. 2009.
[45] C.-L. Tsai, G.-C. Fan, and Y.-S. Lee, "Effects of strain-compensated AlGAN/InGaN superlattice barriers on the optical properties of InGaN light-emitting diodes," *Appl. Phys. A*, vol. 104, no. 1, pp. 319–323, Nov. 2010.
[46] J. Zhang and N. Tansu, "Improvement in spontaneous emission rates for InGaN quantum wells on ternary InGaN substrate for light-emitting diodes," *J. Appl. Phys.*, vol. 110, no. 11, pp. 113110-1–113110-5, Dec. 2011.
[47] P. S. Hsu, M. T. Hardy, F. Wu, I. Koslow, E. C. Young, A. E. Romanov, K. Fujito, D. F. Feezell, S. P. DenBaars, J. S. Speck, and S. Nakamura, "444.9 nm semipolar (1122) laser diode grown on an intentionally stress relaxed InGaN waveguiding layer," *Appl. Phys. Lett.*, vol. 100, no. 4, pp. 021104-1–021104-4, Jan. 2011.